NRC Publications Archive
Archives des publications du CNRC

Characterization of carrier states in CuWO4 thin-films at elevated temperatures using conductometric analysis

Gonzalez, Carlos M.; Dunford, Jeffrey L.; Du, Xiaomei; Post, Michael L.

This publication could be one of several versions: author's original, accepted manuscript or the publisher's version. / La version de cette publication peut être l'une des suivantes : la version prépublication de l'auteur, la version acceptée du manuscrit ou la version de l'éditeur.

For the publisher's version, please access the DOI link below./ Pour consulter la version de l'éditeur, utilisez le lien DOI ci-dessous.

NRC Publications Record / Notice d'Archives des publications de CNRC:
https://nrc-publications.canada.ca/eng/view/object/?id=90b48cb0-8dc6-4ee8-8791-1c1c7ac31811
https://publications-cnrc.canada.ca/fra/voir/objet/?id=90b48cb0-8dc6-4ee8-8791-1c1c7ac31811

Questions? Contact the NRC Publications Archive team at
PublicationsArchive-ArchivesPublications@nrc-cnrc.gc.ca. If you wish to email the authors directly, please see the first page of the publication for their contact information.

Vous avez des questions? Nous pouvons vous aider. Pour communiquer directement avec un auteur, consultez la première page de la revue dans laquelle son article a été publié afin de trouver ses coordonnées. Si vous n'arrivez pas à les repérer, communiquez avec nous à PublicationsArchive-ArchivesPublications@nrc-cnrc.gc.ca.

National Research Council Canada

Conseil national de recherches Canada

Canada

Characterization of Carrier States in $CuWO_4$ Thin-Films at Elevated Temperatures Using Conductometric Analysis

C.M. Gonzalez,* J.L Dunford, X. Du, and M.L. Post

Energy Mining and Environment Portfolio, National Research Council of Canada, 1200 Montreal Road, Ottawa, Ontario K1A 0R6

Abstract: $CuWO_4$ thin-films were deposited by pulsed laser deposition onto an insulating substrate. The temperature dependence of the electronic conductivity of $CuWO_4$ thin-films was determined over the 100 °C - 500 °C temperature range in a synthetic air atmosphere. Additionally, variations of conductivity at 300 °C and 500 °C have been measured for oxygen partial pressures (0.1 atm < $p(O_2)$ < 0.9 atm) in nitrogen. The apparent activation energy ΔE_a for the electrical conduction has been estimated. The study of the temperature effect on the electron transport properties of $CuWO_4$ thin-films reveals the operation of two temperature-dependent oxygen states. The effect of varying oxygen concentration on the electronic properties is discussed in detail. The electrochemical nature of the operating oxygen states for the 100 °C - 500 °C temperature range is deduced using a physicochemical model that relates electronic conductivity with oxygen partial pressure and temperature.

Keywords:
semiconducting metal-oxide, surface characterization, electron transport, conductometric analysis, activation energy, oxygen states.

1. Introduction

The physicochemical characterization of semiconductor materials and, in particular, the material surface characterization, is a fundamental tool for the optimization of the performance of the devices and technologies that have a working principle based on the electronic conduction of semiconducting materials, *e.g.* catalysts, photovoltaics, diodes, transistors, electronic circuits such as printed circuit boards, chemical sensors and transducers. Since these technologies exploit mechanisms that operate through, or near, the semiconducting surface, performance optimization requires comprehensive characterization of the interacting interface [1-2].

* Corresponding author. Tel.: +1 16136686811; fax: +1 16139912384.
E-mail address: carlosmiguelgg@yahoo.com (C.M. Gonzalez).

The electron transport properties of semiconducting metal oxides (thin and thick films) are commonly dependent on both intrinsic and extrinsic structural parameters, temperature and, in general, surface interaction with reactive gas-phase species. In particular, oxygen species (O^{-n}) produced through chemisorption of molecular oxygen have been found to influence strongly the charge transport mechanism and surface reactivity toward redox species. Temporal changes in the electrochemical nature of semiconducting materials, and in particular metal-oxide surfaces, are originated in *i)* electron transfer events promoted by the surrounding gas-phase species (chemisorption and, in general, surface chemistry), *ii)* formation of surface states such as holes, oxygen vacancies and diffusive electrons (temperature effect), *iii)* diffusion of bulk defects to the surface and migration of surface states to the bulk (temperature effect and chemistry) and *iv)* segregation of lattice oxygen at high temperatures [1,3-5]. In particular, the formation of oxygen species arising from chemisorption of molecular oxygen promotes significant changes in surface electrochemical potential. This process yields temperature-dependent oxygen species (*e.g.* O_2^-, O^-, O^{2-}) that exist as a result of both the adsorption of molecular oxygen and electron transfer reactions. Oxygen species promote the operation of electrical fields in the metal-oxide surface, modify charge carrier concentration, cause bending of the conduction level and shifts in the energy of Fermi electrons near the metal-oxide surface [3-13].

Experimental techniques which are applied to surface characterization of semiconducting metal-oxides comprise the phenomenological approach (*e.g.* impedance spectroscopy and conductometry) [10-15], spectroscopic techniques such as X-ray photoelectron spectroscopy (XPS), IR and Raman spectroscopies, electron paramagnetic resonance (EPR) [16-21], and imaging such as transmission electron (TEM) and scanning electron microscopies (SEM) [22-25]. In the present work, conductometric analysis is used to characterise the oxygen states operating in $CuWO_4$ thin-films in the 100 °C < T < 500 °C temperature range and under varying O_2 partial pressure.

2. Experimental

2.1. Materials

$CuWO_4$ was prepared using a solid state reaction of a molar ratio of reactants $CuO : WO_3$ = 1 : 1. The reagents were used as received, WO_3 (Alfa Aesar, 99.998 %) and CuO (Alfa Aesar, 99.995 %). Sintering of the reaction mixture was carried out at 600 °C for 12 hours under flowing O_2. Compacted pellets of $CuWO_4$ for use in film deposition were prepared by isostatic pressing (2 Tonnes) in a mold, followed by sintering at T = 680 °C for 24 hours in flowing O_2.

Thin-films of $CuWO_4$ were prepared from the pellets using the pulsed laser deposition technique (PLD).Thin-films were grown on single crystal sapphire substrates, α-Al_2O_3 $(1\bar{1}02)$, using a Lambda Physik LPX305i laser. The operational conditions of the PLD process are described in detail elsewhere [26], and are summarized in Table 1. Films of approximate thickness ~ 200 nm were deposited and the thickness determined using profilometry (XP-2^{TM} Stylus Profilometer, Ambios Technology, Inc.).

Table 1. Laser deposition parameters for the preparation of $CuWO_4$ nanometric films.

Laser Deposition Parameters	
Excimer Gases :	Krypton-Fluorine
λ :	248 nm
Fluence:	1.5 J / cm^2
Pulse Duration :	20 ns
Pulse Rate :	8 Hz

2.2. Physicochemical Characterization

The laser target ($CuWO_4$) and thin-films were characterized by X-ray diffraction (XRD) using a Bruker-D8 diffractometer with unmonochromated cobalt radiation ($\lambda K\alpha_1$ = 1.78897 Å) and parallel beam geometry. The sample holder was stationary with both the XR-source tube and detector mobile. Phase determination was done by reference to

standard XRD patterns provided in the ICDD **P**owder **D**iffraction **F**ile **D**atabase (supplied as PDF-2 and compiled into DIFFRACT*plus* Reference Database released in 2002).

Specimens were then examined using a JEOL 840A scanning electron microscope. All micrographs were obtaining using an accelerating voltage of 20 kV and a working distance of 15 mm.

The system for evaluating the electronic conductance of the films consisted of a custom-built computer-controlled system with a resistive heater (power supply Xantrex HPD 60-5), gas-supply manifold (MKS Type 1479A Mass-Flo® controllers) and Au contact electrodes connected to a Keithley-2400 SourceMeter. For conductometric studies, gold electrode pads were deposited onto the thin-films using a thermal vacuum deposition procedure (Denton DV502A system) to ensure ohmic contact to the measurement system electrodes. The electronic conductance (σ) was monitored to detect changes in the electron transport properties of the thin-films with changes in experimental conditions (*e.g.* temperature and $p(O_2)$). The gas sources for the measurements were high purity O_2 (Linde, 4.5 grade) and N_2 (Linde, 5.0 grade). Conductance was measured in two sets of experiments, initially with constant O_2 concentration (pO_2 = 0.2 atm, balance N_2) with varying temperature (100 °C < T < 500 °C), and then under two isothermal conditions (T = 300 °C and 500 °C) with varying O_2 partial pressure (0.1 < $p[O_2]$ < 0.9 atm). For all of the experiments, the total gas flow rate was 250 cm^3 / minute, and the total pressure, 1atm.

Prior to initiating conductometric measurements, the thin-films were annealed (T = 520 °C) in the test chamber for 48 hours under dry synthetic air (20 % O_2 in N_2) to eliminate the interference of foreign surface adsorbates such as surface species arising from interaction with water vapor, CO_2, CO, *etc*. The annealing treatment also offered a means to annihilate unstable lattice defects that frequently form during thin-film growth, and allows the equilibration of the semiconducting thin-film with the background gas, thus promoting signal reproducibility. The thin-films were kept in the measurement chamber under dry synthetic air or the other O_2/N_2 mixtures for the duration of the experiments.

3. Results and Discussion

3.1. Structural Characterization

Figure 1 shows the XRDs for (**1a**) a representative $CuWO_4$ thin-film, (**1b**) the PLD $CuWO_4$ target and (**1c**) the substrate α-Al_2O_3 $(1\bar{1}02)$. The formation of single phase $CuWO_4$ was confirmed by comparing the XRDs for both the reaction product and the PLD pellet with those from the database standard DIFFRACT^{plus} – 2002 ($CuWO_4$ standard ID # 01-088-0269). No reflections from reagents were observed. The XRD for the PLD target ($CuWO_4$), **Figure 1b**, displays the characteristic wolframite (triclinic) pattern. As expected, the thin-film XRD (Fig. **1a**) shows the substrate reflections. Since both the substrate (α-Al_2O_3) and the thin-film material ($CuWO_4$) display XRD patterns with reflections about similar 2θ angles, an overlap for some of the diffraction peaks occurred, specifically at $2\theta \approx 26.9$ ° and 62.1 °. This assessment is supported by a change in the observed order of intensity for the reflections arising from the substrate (compare **Figure 1a** with **1c**). The thin-film XRD (Fig. **1a**) displayed a reduced number of reflections compared with the bulk material. This suggests the formation of a $CuWO_4$ film with a preferential orientation.
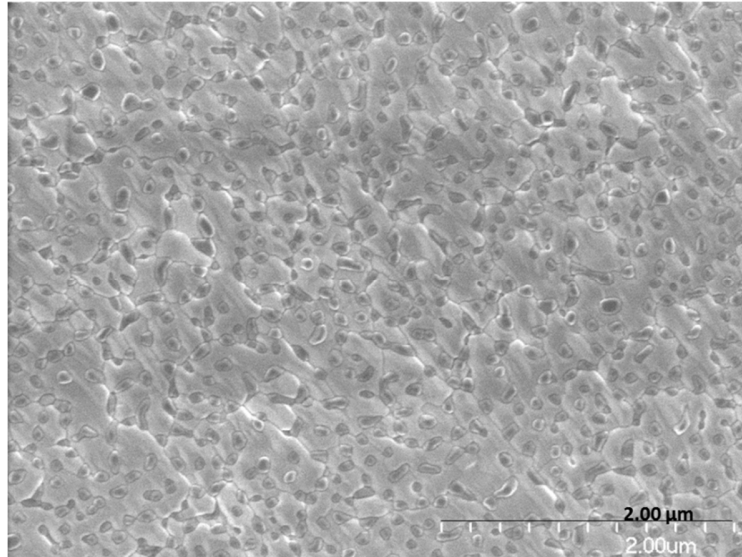
Figure 1. XRD spectra for (1a) a representative CuWO$_4$ thin-film, (1b) the CuWO$_4$ PLD target and, (1c) substrate α-Al$_2$O$_3$ $(1\bar{1}02)$.
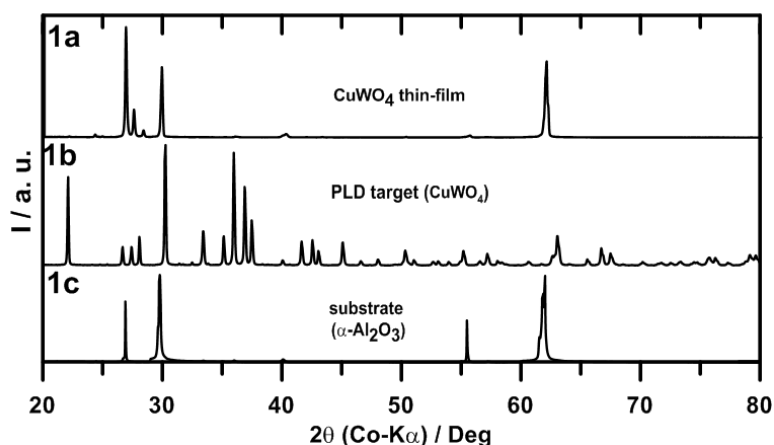
Scanning electron micrographs were obtained for a $CuWO_4$ thin-film, **Figure 2**. The micrograph shows distorted and elongated particles (5 nm to 100 nm) in contact

3.2.1. Temperature Effect on the Electron Transport Properties of CuWO$_4$ Thin-Films

The electrical conductivity of semiconducting materials is a thermally activated process. Although transport of charge carriers across the semiconductor surface is a complex process, the electron transport dynamics is satisfactorily described by **Equation 1** [5-10,12-15,22,27-33]. This equation relates electronic conductivity (G) with temperature by means of an Arrhenius-like relationship ($ln\ G \propto -\frac{1}{T}$) **Equation 1**, G^* is an entropic parameter accounting for i) the granular morphology (grain size-distribution, quality of inter-grain contacts, crystal structure, lattice defects and surface states), ii) field effects arising from the coulombic charge of both the charge carriers and surface states (including oxygen states O^{n-}), and iii) electron-lattice interactions [3-7,12,14,29,33]. G^* is also a parameter that includes the influence on the surface by the gas-phase surroundings and accounts for the concentration of reactive gas-phase species (*e.g.* O_2, CO, CO_2, NO_x, H_2O, *etc.*). ΔE_a represents the energy required for the promotion of an electron in the proximity of the Fermi level (under the electrostatic

influence of surface states, including oxygen species) to a diffusive state, and k_B is the Boltzmann's constant.

$$G = G^* \exp\left(-\frac{\Delta E_a}{k_B T}\right)$$ **(1)**

Differentiation of **Equation 1** in logarithmic form (*ln G*) with respect to reciprocal temperature ($\frac{1}{T}$) yields **Equation 2**, which facilitates estimation of the activation energy ΔE_a for electronic conduction.

$$\frac{\partial \ln \sigma}{\partial \frac{1}{T}} = -\frac{\Delta E_a}{k_B}$$ **(2)**

Equation 2 lists conductance σ instead of conductivity *G*. Within Drude's model of electronic conduction, the conductivity G_D and the conductance σ are related by **Equation 3**, where *A* represents the cross-section of the conducting material and ℓ, the corresponding length.

$$G_D = \sigma \frac{A}{\ell}$$ **(3)**

Parameters *A* and ℓ (**Equation 3**) can be considered to be nearly independent of temperature (that is, for materials with small coefficient of thermal expansion, which is often the case for ceramics). Substitution of *G* by the related parameter σ (**Equation 3**) in the derivative of **Equation 1** with $\frac{1}{T}$ (that is, $\frac{\partial \ln G}{\partial \frac{1}{T}}$) leads to **Equation 2**.

Figure 3 (*ln R* vs. $\frac{1}{T}$, where R is the measured resistance) shows the temperature effect (100 °C < *T* < 500 °C range) on the electron transport dynamics of a $CuWO_4$ thin-film in dry synthetic air (20 % O_2 in N_2). The electronic conductance (σ) increased with temperature (*ln R* increased with $\frac{1}{T}$), which agrees with the thermally activated nature of the electron conductivity in semiconducting materials. The Arrhenius

plot in **Figure 3** shows two distinct temperature domains. These domains are characterized by a change in slope of the plot with an onset temperature, in this case T ~ 250 °C. For the thin-films under investigation, the temperature-dependent domains appear within 100 °C < T < 250 °C with ΔE_a = 0.34 eV, and within 250 °C < T < 500 °C with ΔE_a = 0.17 eV. The lower activation energy ΔE_a found for the latter temperature range has been explained as a result of the increase in the number of charge carriers caused by an increasing number of unstable lattice oxygen atoms [1,7,9-10,12,19,21,27]. Similar transition temperatures for electronic conduction have been previously reported for $CuWO_4$ thin-films; *i.e.* transition temperature T ~ 200 °C, ΔE_a =0.57 eV for the 37 °C < T < 200 °C temperature range, and ΔE_a = 0.12 eV for the 200 °C < T < 340 °C temperature range [23]. The temperature dependence of activation energy for electronic conduction ΔE_a has been explained as a consequence of varying field effects in the semiconductor surface [29,33-45]. The electrochemical changes that the interacting interface undergoes with temperature result in the operation of temperature-dependent field effects. The variation in surface electrochemical potential is related to *i*) a change in the electrochemical nature of oxygen species with temperature ($O_2 \rightarrow O_2^- \rightarrow O^- \rightarrow O^{2-}$), and an associated variation in surface charge and number of conduction electrons, *ii*) the coulombic interaction between conduction electrons and oxygen states (formation of a depletion layer and band bending), *iii*) the reversibility of oxygen chemisorption (destabilization of chemical bonding with increasing temperature, *e.g.* desorption of oxygen states resulting in a rise in the number of surface electrons and a corresponding change in surface charge), *iv*) an increase in the segregation of lattice oxygen atoms and migration of oxygen vacancies from the bulk to the surface with increasing temperature, and *v*) the effect of temperature changes on the electron-lattice interactions (*e.g.* increase in the electron scatter with temperature) [46]. For instance, for WO_3 thin-films, it has been reported that O_2^- adsorbates are stable below 150 °C and coexist with HO^- surface species; at higher temperatures, O_2^- adsorbates undergo stepwise reduction to O^- (stable in the 150 °C < T < 300 °C range). As temperature continues to increase, O^- will further reduce to O^{2-}, which is stable above T ~ 300 °C [40]. Whereas for SnO_2 thin-films, water and O_2^- adsorbates are stable in the 80 °C < T < 180 °C temperature range, O^-, between 180 °C

and 500 °C, and O^{2-} above 500 °C [35,39,47-48]. Based on these findings, the temperature ranges in Figure 2 can be explained as being a result of the formation of two different oxygen states as temperature increases.

Figure 3. Temperature effect ($ln\ R$ vs. $\frac{1}{T}$) on the electronic resistance R of a CuWO$_4$ thin-film for the 100 °C < T < 500 °C temperature range under synthetic air (20 % O$_2$ in N$_2$).
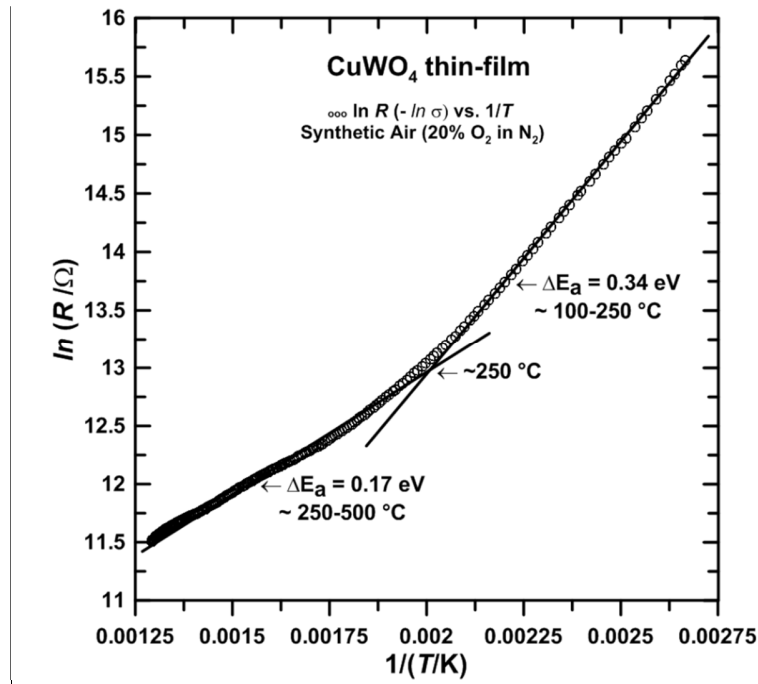
The temperature dependence found for ΔE_a (**Figure 3**) could also be related to chemical and structural changes in the thin-film with increasing temperature such as bulk changes in the crystal lattice or formation of oxygen-depleted phases. However, the formation of oxygen-depleted phases (CuWO$_{4-\delta}$) as temperature increases is not likely to arise in the temperature range studied since the process would produce a significant change in the electron conduction profile with temperature (which would likely result in a discontinuity in the relationship of conductance with temperature, and in the evolution of a metallic-regime for conductivity as a result of the formation of an extensive intrinsic doping) [49]. Moreover, the resulting oxygen loss will produce the parallel reduction of W^{6+} (or Cu^{2+}) because charge balance requires that for each oxygen vacancy V_O^{2+}, two W^{6+} (or two Cu^{2+}) centres convert to two W^{5+} (Cu^+) centres.

This process involves a substantial reorganization of the electron density and significant changes in bonding parameters and crystal lattice. Consequently, the changes in both coulombic and structural parameters will impede the return to the conductance value corresponding to a predetermined reference state (defined in this study for the stoichiometric single phase $CuWO_4$ in synthetic air 20 % O_2 in N_2). This situation did not arise for the experiment summarized in **Figure 3**. Another factor to consider is a phase transition near the frontier temperature (for the case studied $T \sim 250$ °C). However, $CuWO_4$ does not undergo a lattice transformation in the temperature range studied [50].

3.2.2. Characterization of Operating Oxygen Sates by Conductometric Analysis

Equations 4 and **5** summarize the formation of the oxygen species in semiconducting metal oxide surfaces [4-6,31,48]. In the model below, O_0^x represents an unstable lattice oxygen, V_O^{n+} a single or double ionized oxygen vacancy, and $O^{n'-}$, the corresponding oxygen species (O_2^-, O^-, O^{2-}).

$$O_0^x \quad \rightleftarrows \quad \tfrac{1}{2} O_2 + V_O^{n+} + n\,e^- \tag{4}$$

$$\tfrac{1}{2} O_2 + n'e^- \rightleftarrows O^{n'-} \tag{5}$$

Equation 5 defines the effect of oxygen chemisorption on the electronic conduction of n-type metal-oxide materials, which is manifested through a reduction in electronic conductance with increasing $[O_2]$. The electronic conductivity G relates to the number of effective charge carriers through **Equation 6**, where $[e^-]$ is the concentration of charge carriers that participate in electronic conduction assuming that the contribution of positive charge carriers to the electric conductance is negligible, μ denotes the electron mobility and e, electronic charge [38-39,42-43]. **Equation 6** shows the relationship of electronic conductivity G with the charge carrier concentration $[e^-]$ and reveals that a reduction in the number of surface electrons as a result of oxygen chemisorption (**Equation 5**) leads to a decrease in surface conductivity. For the temperature range investigated (300 °C < T < 500 °C), the expected oxygen species $O^{n'-}$ are O^- or O^{2-}

[22,33,35,39-40,47,49-51]. The charge conduction mechanism has been considered to occur through electron conduction since typically mixed ionic-electronic conduction occurs at higher temperatures ($T > 700$ °C) which promotes the formation of a significant number of oxygen vacancies (V_O^{2+}) and the formation of oxygen depleted phases with mixed valence states [51-52].

$$G_D = [e^-]\mu e \tag{6}$$

Equation 7 has been used previously to evaluate the effect of oxygen concentration on the electronic conductivity of semiconducting metal-oxides [37,45,52-57]. In the model, pO_2 is the oxygen partial pressure, n relates to the number of charge carriers that participate in the electronic conduction as indicated in **Equation 4**, ΔE_a is, as before, the apparent activation energy for conduction. G' is considered a constant, temperature-independent term, with the same physical meaning as G^* outlined in **Section 3.2.1** (**Equation 1**), except that in this case G' is a parameter independent of the concentration of reactive gas-phase species. It has been established that the electron conductivity of n-type semiconducting metal-oxides under the influence of oxygen states in intermediate and high temperature ranges (O^- or O^{2-}) is primarily controlled by the rate for promotion of electrons to a diffusion state (**Equation 4**) and, to a lesser extent, on the formation of new oxygen states with increasing [O_2], **Equation 5** [39]. Formation of an increasing number of oxygen states with both [O_2] and temperature features a kinetics limitation, which is related to a limited surface for formation of oxygen adsorbates (saturation effect), and electronic repulsion effects (interaction between conduction electrons and negative oxygen species), and a thermodynamic limitation related to both the destabilization of oxygen adsorbates with increasing temperature (which is evidenced by the reduction of effective coverage with temperature), and an increase in oxygen vacancies at high temperature [12,57-61].

$$G = pO_2^{\frac{-1}{2n+2}} G' exp\left(-\frac{\Delta E_a}{k_B T}\right) \tag{7}$$

The slope of a plot for *ln G* (or *ln σ*) vs. *ln p*O_2, **Equation** 8, allows inferring the nature of surface oxygen vacancies V_O^{n+} available for bonding interactions with molecular oxygen and consequently the electrochemical nature of the oxygen species in operation at the investigated temperature range. For the relationship $\frac{\partial\, ln\, G}{\partial\, ln\, pO_2}$, *ln G* can be substituted by *ln σ* since the thin-film cross-section, *A*, and length, ℓ , both relating *G* with σ (defined in **Equation 3**), are not parameters of the O_2 concentration.

$$\frac{\partial\, ln\, \sigma}{\partial\, ln\, pO_2} = \frac{-1}{2n+2} \tag{8}$$

Since the oxygen vacancies (V_O^{n+}) are ideal structural sites for the accommodation of oxygen species ($O^{n'-}$), it is reasonable to consider that oxygen bonding interactions take place through an intermediate of such surface defects. Therefore, the electrochemical nature of the oxygen-states can be reasonably inferred from the charge of operating oxygen vacancies at a given temperature (**Equation 4**) [62]. Based on these considerations, the electrochemical nature of majority oxygen-species can be related to the electrochemical nature of surface vacancies. The equilibrium constant K_e, **Equation 9**, for the process represented in **Equation 4** offers a simple means to evaluate the effect of surrounding O_2 on the electrochemical nature of oxygen states [39,42-43,51,63]. Lattice oxygen concentration $[O_O^x]$ is not considered for the estimation of K_e since the corresponding concentration in equilibrium with gas-phase species is approximately constant at any given $[O_2]$ (ratio for number of O_O^x to lattice volume ≈ constant).

$$K_e = \left[V_O^{n+}\right]\left[e^-\right]^n pO_2^{1/2} \tag{9}$$

Based on **Equation 4,** the mass-action law for formation of charge carriers requires that the ratio $[V_O^{n+}]$ to $[e^-]_{cond}$ equals $\frac{\left[V_O^{n+}\right]}{\left[e^-\right]_{cond}} = \frac{1}{n}$, which allows rewriting **Equation 9** into **Equation 10**. This equation establishes an inverse relation between the

concentration of effective charge-carriers [e^-] and oxygen concentration ($pO_2{}^{-m}$) for n-type semiconductors.

$$[e^-]_{cond} = K_e\, pO_2{}^{\frac{-1}{2n+2}}$$ (**10**)

Based on **Equations 4** and **5**, the formation of oxygen species ($O^{n'-}$) requires an interaction of majority oxygen vacancies ($V_O{}^{n+}$) with surrounding molecular O_2 and the removal of an equivalent number of electrons (*n*). Thus, the formation of O^- will require the interaction of O_2 with a single ionized vacancy ($V_O{}^+$) and consumption of a chemical equivalent of electrons e^- (*n* = 1). Therefore, for a system where the majority oxygen state is O^-, the slope *(S$_l$)* for the corresponding plot for *ln* σ vs. *ln* pO_2 should be equal to $-\frac{1}{4}$ (as indicated in **Equation 8**, with *n = 1*). Similarly, if O^{2-} were the resulting oxygen-state upon interaction between surrounding O_2 and predominant double ionized oxygen vacancies ($V_O{}^{2+}$), then *n* = 2, and therefore the slope of a plot *ln* σ vs. *ln* pO_2 should be $-\frac{1}{6}$. Based on this, the study of the effect of [O_2] on the surface conductance will allow evaluating the electrochemical nature of the operating oxygen states at constant temperature.

      Figure 4 shows the dependence of resistance (*ln R*) with the concentration of surrounding molecular oxygen (*ln* pO_2) in N_2 at 300ºC and 500 °C (total pressure 1atm). The resistance *R* data for both temperatures can be defined as having a linear relationship to *ln* pO_2 both with similar slopes (S$_l$), *i.e.* S$_l$ (300 °C) = – 0.23 ± 0.06, and S$_l$ (500 °C) = – 0.26 ± 0.04. These values as applied to the **Equation** 8 yield *n* ≈ 1 (as shown above, a slope of S$_l$ ~ 0.25 implies that the oxygen state $O^{n'-}$ in dynamic interaction with the surrounding molecular O_2 is O^-). The increasing resistance values (*ln R*) with O_2 (*ln* pO_2) is an indication of the n-type conductivity for the $CuWO_4$ thin-films.

      When differentiating **Equation 7,** the effective charge carrier mobility *μ* (defined in **Equation 6**) was considered to be independent of temperature, which is not strictly

true since $\mu \propto exp\left(-\dfrac{E_\mu}{k_B T}\right)$, where E_μ is the activation energy for electron mobility.

Nonetheless, for the present case this is a valid assumption, since the activation energy for mobility E_μ of n-type semiconducting metal oxides is smaller than the activation energy for conduction ΔE_a, usually by an order of magnitude [43,49,62]. For instance, in the case of bulk samples of oxygen-depleted tungsten oxides ($WO_{3-\delta}$), the estimates of corresponding activation energies for E_μ using Hall mobility have been reported in the 0.01 eV $< E_\mu <$ 0.06 eV range, whereas for the same samples, the activation energy for electronic conduction was in the range $\sim$ 0.1 eV $< \Delta E_a <$ 0.2 eV [49].

Figure 4. Effect of increasing O_2/N_2 concentration ($\sim$ 0.1 $< pO_2 <$ 0.9 atm) on the electronic resistance (R) of a $CuWO_4$ thin-film under varying ratio for O_2-to-N_2. The total pressure for all measurements was 1 atm ($pO_2 + pN_2$ = 1 atm).
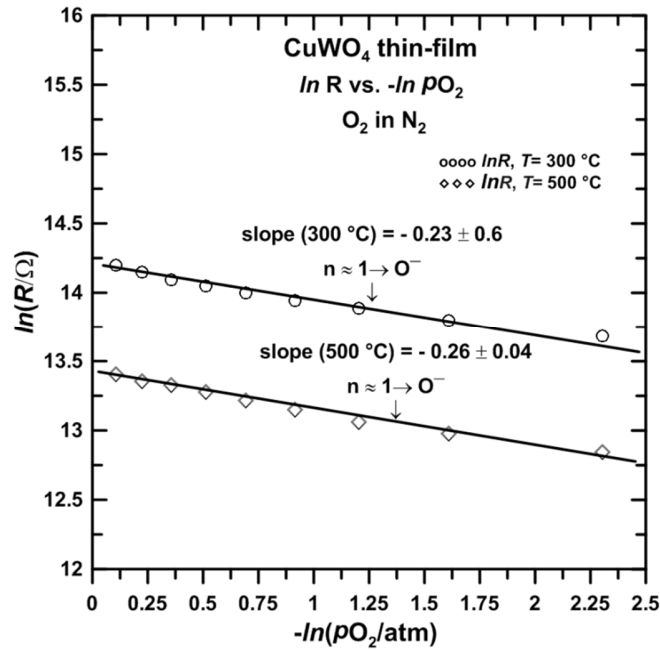
Since the operation of mixed conduction mechanisms usually produces sigmoid isotherms for plots of $ln\ \sigma$ vs. $ln\ pO_2$ [40,52,62,65-67], the linearity of the relationship between $ln\ R$ and $ln\ pO_2$ for the isotherms in Figure 3 provides further evidence of the operation of a charge conduction mechanism through diffusive electrons. The evaluation of the nature of oxygen states ($O^{n'-}$) for the thin-films under investigation using conductometry illustrates the potential of the method for studying semiconducting

interfaces and, by extension, for the study of surface reactions in catalytic processes that proceed through the intermediation of oxygen states $O^{n'-}$. The reasonable fit also suggests that the $CuWO_4$ films under study are free of impurities and that the semiconducting metal-oxide surface reaches equilibrium with the surrounding gas during measurement. In agreement with the temperature domains established using the Arrhenius plot **Figure 3 (**which predicts the operation of two consecutive temperature-dependent oxygen states $O^{n'-}$, that is, a majority oxygen state that operates in the 100 °C < T < 250 °C range, and another majority oxygen state in the 250 °C < T < 500 °C range), O^- was the operating oxygen state identified at both $T \sim 300$ °C and $T \sim 500$ °C. Based on the results summarized above and other literature reports, the oxygen state operating in the 100 °C < T < 250 °C range can be assigned to O_2^- [22,33,35,40].

4. Conclusions

The qualitative description of surface species in semiconducting $CuWO_4$ thin-films was carried using a model frequently invoked for the oxygen chemisorption process in n-type semiconducting metal-oxide surfaces. As established in a number of studies, the electronic conductance was satisfactorily characterized as a parameter of the oxygen concentration ($G \propto pO_2^m$, where $m = \dfrac{-1}{2n+2}$) [39-64]. In agreement with these reports, for the study under discussion the oxygen state O^{n-} operating in the intermediate-high temperature range (300 °C < T < 500 °C) was O^-. The agreement between theory and experiment indicates that, in the absence of moisture and other gas-phase species, the mode of charge conduction is through diffusive electrons, allowing eliminating a significant contribution from other charge conduction mechanisms (*e.g.* ionic conductivity, protonic conduction).

This approach is an example of the use of a macroscopic property for characterising chemisorbed species at the molecular level. Utilization of the physical model outlined herein for the characterization of extrinsic surface states, and, in particular, oxygen species requires the use of a single-phase semiconducting metal oxide. This work provides support for using conductometric analysis to study surface

states as a complementary technique to the spectroscopic characterization of semiconducting metal-oxide interfaces.

Acknowledgements

Bibliography:

[1]   S. M. Sze, M.-K. Lee, Semiconductor Devices: Physics and Technology. John Wiley & Sons, 2012.

[2]   H.L. Tuller, S.J. Litzelman, G.C. Whitfield, Chapter 10 Electrical Conduction in Nanostructured Ceramics. (Eds. R. Riedel, I.-W. Chen, Ceramics Science and Technology, Materials and Properties 2) Wiley-VCH, 2010.

[3]   D. K.Aswal, Sh. Gupta, K. (Eds.) Science and Technology of Chemiresistors Gas Sensors. Nova Science Publishers, Inc. 2007.

[4]   G. Pacchioni, ChemPhysChem. 4 (2003) 1041-1047.

[5]   V.E. Bochenkov, G.B. Sergeev, Adv. Colloid Interface Sci. 116 (2005) 245-254.

[6]   H. Statz, G. A. Demars, Phys. Rev. 111 (1958) 169-182.

[7]   N. Barsan, D. Koziej, U. Weimar, Sens. Actuators, B. 121 (2007) 18-35.

[8]   Q. Fu,T. Wagnera, Surf. Sci. Reports 62 (2007), 431-498.

[9]   C. Malagu , V. Guidi, M. Stefancich, M.C. Carotta, G. J. Mertinelli, Appl. Phys. 91 (2002) 808-814.

[10] A. Varpula, S. Novikov, A. Haarahiltunen, P. Kuivalainen, Sens. and Actuators, B 159 (2011) 12-26.

[11] H. Geistlinger, Sens. Actuators, B 7 (1992) 619-625.

[12] T. A. Goodwin, P. Mark, Prog. Surf. Sci. 1 (1971) 1-64.

[13] T. Sahm, A. Gurlo, N. Bârsan, U. Weimar, Sens. Actuators B 118 (2006) 78-83.

[14] H. Geistlinger, Surf. Sci. 277 (1992) 429–441.

[15] S. A. Bilmes, D. Posadas, Colloids Surf. A 134 (1998) 47-57.

[16] J.-Ch. Dupin, D. Gonbeau, P. Vinatier, A Levasseur, Phys. Chem. Chem. Phys. 2 (2000) 1319-1324.

[17] D. Cappus, M. Menges, C. Xu, D. Ehrlich, B. Dillmann, C. A. Ventrice, J. Libuda, M. Bäumer, S. Wohlrab, F. Winkelmann, H. Kuhlenbeck, H.-J. Freund, J. Electron. Spectrosc. Relat. Phenom. 68 (1994) 347-355.

[18] D. Cappus, M. Haßel, E. Neuhaus, M. Heber, F. Rohr, H.-J. Freund, Surf. Sci. 337 (1995) 268-277.

[19] A. P. Shpak, A. M. Korduban, M. M. Medvedskij, V. O. Kandyba, J. Electron. Spectrosc. Relat. Phenom. 156-158 (2007) 172-175.

[20] A.F. Carley, P.R. Davies, M.W. Roberts, Catal. Today 169 (2011) 118-124.

[21] T. Herranz, X. Deng, A. Cabot, M. Salmeron, J. Catal. 283 (2011) 119-123.

[22] M. Batzill, U. Diebold, Prog. Surf. Sci. 79 (2005) 47-154.

[23] P. K. Pandey, N.S. Bhave, R.B. Kharat, Mater. Lett. 59 (2005) 3149-3155.

[24] J.-H. Lee, Sens. Actuators B 140 (2009) 319-336.

[25] G. Korotcenkov, Mater. Sci. Eng. R 61 (2008) 1-39.

[26]   Copper Tungstate Thin-films for Nitric Oxide Sensing. C.M.Gonzalez, X Du, J.L. Dunford, M.L. Post, Sens. Actuators B: Chem. (2012), http://dx.doi.org/10.1016/j.snb.2012.06.067.

[27]   T. Ando, Rev. Mod. Phys. 54 (1982) 437-672.

[28]   P. A. Lee, Rev. Mod. Phys. 57 (1985) 287-337.

[29]   K. Aguir, C. Lemire, D.B.B. Lollman, Sens. Actuators B 84 (2002) 1-5.

[30]   D. Baresel, W. Gellert, W. Sarholz, P. Scharner , Sens. Actuators 6 (1984) 35-50.

[31]   M. J. Sienko, P. F. Weller, Inorg. Chem. 1 (1962) 324-331.

[32]   Sahle, W.; Nygren, M. J. Solid State Chem. 48 (1983) 154-160.

[33]   J.Ding, T.J. McAvoy, R.E. Cavicchi, S. Semancik, Sens. Actuators B 77 (2001) 597-613.

[34]   J. Guérin, K. Aguir, M. Bendahan, Sens. Actuators B 119 (2006) 327-334.

[35]   D. Kohl, Sens. Actuators B 18 (1989) 71-113.

[36]   G. Korotcenkov, B.K Cho, Sens. and Actuators B 142 (2009) 321-330.

[37]   G. Korotcenkov, Mater. Sci. Eng. B 139 (2007) 1-23.

[38]   S. Saukko, U. Lassi, V. Lantto, M. Kroneld, S. Novikov, P. Kuivalainen, T. Rantala, J. Mizsei, Thin Solid Films 490 (2005) 48-53.

[39]   J. McAleer, P. Moseley, J. Norris, D. Williams, J. Chem. Soc., Faraday Trans. I, 83 (1987) 1323-1346.

[40]   W. Yu-De, C. Zhan-Xian, L. Yan-Feng, Z. Zhen-Lai, W. Xing-Hui, Solid-State Electron. 45 (2001), 639-644.

[41]   K. Wetchakun, T. Samerjai, N. Tamaekong, C. Liewhiran, C. Siriwong, V. Kruefu, A. Wisitsoraat, A. Tuantranont, S. Phanichphant, Sens. Actuators B. 2011 In Press.

[42]   P. T. Moseley, Meas. Sci. Technol. 8 (1997) 223-237.

[43]   N. Bârsan, Sens. Actuators B 17 (1994) 241-246.

[44]   K. Aguir, C. Lemire, D.B.B. Lollman, Sens. Actuators B 84 (2002) 1-5.

[45]   P. T. Moseley, D. E. Williams, Polyhedron 8 (1989) 1615-1618.

[46]   V. E. Henrich, Appl. Surf. Sci. 72 (1993) 277-284.

[47]   F. Hellegouarch, F. Arefi-Khonsari, R. Planade, J. Amouroux, Sens. Actuators B. 73 (2001) 27-34.

[48]   G. Geiland, Sens. Actuators. 2 (1982) 343-351.

[49]   J. M. Berak, M. Sienko, J. Solid State Chem. 2 (1970) 109-133.

[50]   S.K. Arora, T. Mathew, Phys. State Solid 116 (1989) 405-413.

[51]   G. Geiland, Sens. Actuators 2 (1982) 343-351.

[52]   A. Rothschild, W. Menesklou, H. L. Tuller, E. Ivers-Tiffée, Chem. Mater. 18 (2006) 3651-3659.

[53]   P. Bonasewicz, W. Hirschwald, G. Neumann, Appl. Surf. Sci. 28 (1987) 135-146.

[54]   P. T. Moseley, Sens. Actuators B 6 (1992) 149-152.

[55]   N. Yamazoe, K. Shimanoe, Sens. Actuators B 128 (2008) 566-573.

[56]   P. Bonasewicwz, W. Hirschwald, G. Neumann, Phys. Stat. Sol. A 97 (1986) 593-599.

[57]   C. O. Park, S. A. Akbar, J. Mater. Sci. 38 (2003) 4611-4637.

[58]   T. A. Jones, J. G. Firth, B. Mann, Sens. Actuators B 8 (1985) 281-306.

[59]   H. Geistlinger, Sens. Actuators B 17 (1993) 47-60.

[60]   N. Sergent, P. Gélin, L. Périer-Camby, H. Praliaud, G. Thomas, Sens. Actuators B 84 (2002) 176-188.

[61]   Z. M. Jarzebski, J. P. Marton, J. Electrochem. Soc. 123 (1976) 299C–310C.

[62]   Z. M. Jarzebski, J. P. Marton, J. Electrochem. Soc. 123 (1976) 123, 333C–346C.

[63]   S. R. Bishop, T. S. Stefanik, H. L. Phys. Chem. Chem. Phys. 13 (2011) 10165-10173.

[64]   S. R. Morrison, Surf. Sci. 10 (1968) 459-169.

[65]   T. A. Goodwin, P. Mark, Prog. Surf. Sci. 1 (1971) 1-64.

[66]   H. L. Tuller, Sens. Actuators 4 (1983) 679-688.

[67]   Ch. Ohly, S. Hoffmann-Eifert, R. Waser, J. Electroceram. 13 (2004) 599-603.

Figure Captions

Figure 1. XRD spectra for (1a) a representative CuWO$_4$ thin-film, (1b) the CuWO$_4$ PLD target and, (1c) substrate α-Al$_2$O$_3$ $(1\bar{1}02)$.

Figure 2. SEM Micrograph of a CuWO$_4$ thin-film.

Figure 3. Temperature effect ($ln\ R$ vs. $\frac{1}{T}$) on the electronic resistance R of a CuWO$_4$ thin-film for the 100 °C < T < 500 °C temperature range under synthetic air (20 % O$_2$ in N$_2$).

Figure 4. Effect of increasing O$_2$/N$_2$ concentration (~ 0.1 < pO$_2$ < 0.9 atm) on the electronic resistance (R) of a CuWO$_4$ thin-film under varying ratio for O$_2$-to-N$_2$. The total pressure for all measurements was 1 atm (pO$_2$ + pN$_2$ = 1 atm).